Journal of Quantitative Spectroscopy & Radiative Transfer ▮ (▮▮▮▮) ▮▮▮–▮▮▮

Contents lists available at ScienceDirect

Journal of Quantitative Spectroscopy & Radiative Transfer

journal homepage: www.elsevier.com/locate/jqsrt

A radiative transfer model for an idealized and non-scattering atmosphere and its application for ground-based remote sensing

Marc Schneebeli [a,b,*], Christian Mätzler [b]

[a] EPFL, Environmental Remote Sensing Laboratory, 1015 Lausanne, Switzerland
[b] University of Bern, Institute of Applied Physics, 3012 Bern, Switzerland

ARTICLE INFO

Article history:
Received 18 August 2010
Received in revised form
11 October 2010
Accepted 12 October 2010

Keywords:
Microwave
Ground-based
Radiometry
Profile inversion

ABSTRACT

Inversion of tropospheric profiles from ground-based microwave measurements requires a simple and accurate model for calculating the brightness temperatures as received by the radiometer. In the first part, an analytic solution of the radiative transfer equation is derived for an exponentially decaying absorption coefficient and a linear temperature gradient. Based on the obtained analytic expressions, a discretized radiative transfer scheme is developed in the second part. The new scheme incorporates the generic behavior of the atmosphere with the effect that brightness temperatures can be modeled more accurately and with fewer grid points compared to commonly used radiative transfer schemes. The brightness temperature modeling accuracy was improved by a factor of six. The results suggest that the model could be employed for the retrieval of temperature and humidity profiles.

1. Introduction

Satellite measurements of the troposphere pay for their global or at least large areal coverage with a lack in spatial and temporal resolution. In addition, the relatively dense troposphere increases the difficulties for spaceborne sensors. Therefore, ground-based remote sensors are still a key tool in today's tropospheric research [18]. Microwave radiometers employed in this research field can be used for the retrieval of integrated water vapor (IWV) [5], integrated liquid water (ILW) [9,4] as well as temperature and humidity profiles [2]. In those applications usually no wavelength smaller than 2 mm is used (except for arctic environments with very low humidity [3]), such that scattering can be neglected. The basis of all those retrievals is an accurate and reliable radiative transfer (RT) code. RT codes like ARTS (The Atmospheric Radiative Transfer System) by Bühler et al. [1] fulfill these requirements and are widely used in the remote sensing community.

However, in order to provide a general applicability, these codes do not take the generic structure of the troposphere (exponential decay of absorption coefficients with height, linear decay of the temperature) into account. Another problem comes with a change of the observation angle. In ground-based remote sensing, often a plane-parallel atmosphere is assumed. If the observation angle gets changed, one could simply modify the opacities with the well-known relation $\tau(\theta) = \tau(0)\sec(\theta)$, with $\tau(\theta)$ being the opacity under the zenith angle θ and $\tau(0)$ being the zenith opacity. But in highly absorbing media, this often leads to high opacities in the single atmospheric layers of the model. Therefore, the atmosphere needs to be discretized on a finer grid with more layers of smaller vertical extent to achieve results of sufficient accuracy.

In the first part of this chapter, the atmosphere's generic structure is incorporated in the radiative transfer equation (RTE), leading to an analytic radiative transfer model of a simplified atmosphere. The analytic expressions that were derived in this manner are used afterwards for numerical

* Corresponding author at: EPFL, Environmental Remote Sensing Laboratory, 1015 Lausanne, Switzerland.
E-mail address: marc.schneebeli@epfl.ch (M. Schneebeli).

0022-4073/$ - see front matter © 2010 Elsevier Ltd. All rights reserved.
doi:10.1016/j.jqsrt.2010.10.018

modeling of brightness temperatures in realistic atmospheres. The accuracy is assessed for different frequencies, zenith angles and sampling grid sizes.

An extensive study on the accuracy of clear sky atmospheric microwave RT models was already done by Melsheimer et al. [12], where different models and their implementation of spectroscopic line shapes, absorption coefficients and the general RT calculation for different geometries were compared. Our focus differs from the mentioned article in the way that the interest is put on the implementation of the numerical RT calculation and the choice of the calculation grid. The choice of a retrieval grid is a delicate task in atmospheric profiling, since a trade-off between computation time and brightness temperature accuracy has to be made. Some of these questions are addressed in Section 4.

2. The RTE for an exponentially decreasing and non-scattering atmosphere with a linear temperature profile

Our model troposphere shows an exponential decrease of the absorption coefficients of its constituents with increasing height. Therefore, the absorption coefficient γ_a can be written as

$$\gamma_a(z) = \gamma_a(0) e^{-z/z_0}, \tag{1}$$

where $\gamma_a(0)$ is the value of the absorption coefficient at the surface, z is the height above the surface, and z_0 is a scale height to be chosen. In the troposphere, one can assume the temperature profile $T(z)$ to be linearly decreasing with height z up to the tropopause height z_p. For simplicity, we assume a constant temperature above the tropopause height such that the temperature profile can be written as follows:

$$T(z) = \begin{cases} T_g - \Gamma z; & 0 \le z \le z_p, \\ T_p = T_g - \Gamma z_p; & z_p < z. \end{cases} \tag{2}$$

Here, $-\Gamma$ denotes the temperature gradient, T_g is the temperature at the ground and T_p is the temperature at the tropopause. As a further constraint, we assume the atmosphere to be plane-parallel, such that we can express the zenith opacity as

$$\tau(z) = \int_0^z \gamma_a(z')\, \mathrm{d}z'. \tag{3}$$

Furthermore, we define $\mu = \cos\theta$, with the zenith angle θ. The slant path opacity therefore becomes $\tau(\theta) = \tau/\mu$.

2.1. Downwelling radiation

Now, the integral form of the RTE in the Rayleigh–Jeans approximation for the brightness temperature intercepted at the ground is, e.g. Janssen [8]:

$$T_b(\tau = 0, \mu) = T_{b1} e^{-\tau_p/\mu} + \frac{1}{\mu} \int_0^{\tau_p} T(\tau) e^{-\tau/\mu}\, \mathrm{d}\tau. \tag{4}$$

T_{b1} is hereby the brightness temperature at the tropopause and $\tau_p = \tau(z = z_p)$. With the further definition of $\tau_\infty = \tau(z = \infty)$ and the absorption coefficient defined in (1), we get $\tau = \tau_\infty(1 - e^{-z/z_0})$ and $\tau_\infty = \gamma_a(0) z_0$. Therefore, the height variable z can be expressed as $z = -z_0 \ln(1 - \tau/\tau_\infty)$, and together with (2), the τ dependence of the temperature is written as

$$T(\tau) = T_g + \Gamma z_0 \ln\left(1 - \frac{\tau}{\tau_\infty}\right); \quad 0 \le \tau \le \tau_p. \tag{5}$$

Eq. (4) can now be written as

$$T_b(\tau = 0, \mu) = T_{b1} e^{-\tau_p/\mu} + \frac{1}{\mu} \int_0^{\tau_p} \left(T_g + \Gamma z_0 \ln\left(1 - \frac{\tau}{\tau_\infty}\right)\right) e^{-\tau/\mu}\, \mathrm{d}\tau. \tag{6}$$

Simplifying the above expression with the definitions $\alpha = \tau_\infty/\mu$, $\beta = \tau_p/\mu$ and $x' = \tau/\tau_\infty$, the equation now reads

$$T_b(\tau = 0, \mu) = T_{b\downarrow} = T_{b1} e^{-\beta} + T_g(1 - e^{-\beta}) - \Gamma z_0 \alpha L_\downarrow, \tag{7}$$

where

$$L_\downarrow = -\int_0^x \ln(1 - x') e^{-\alpha x'}\, \mathrm{d}x', \tag{8}$$

with $x = \tau_p/\tau_\infty = \beta/\alpha = 1 - \exp(-z_p/z_0)$. The arrow $\downarrow$ was introduced to indicate the downwelling direction.

Unfortunately there exists no direct analytical solution for $L_\downarrow$. For values being located in the interval $[0 \le x' \le x \le 1]$, we replace the logarithm by its Taylor Series: $\ln(1 - x') = -\sum_{n=1}^{\infty} x'^n/n$, leading to a convergent series of integrals

$$L_\downarrow = \sum_{n=1}^{\infty} L_{n\downarrow}, \tag{9}$$

where

$$\sum_{n=1}^{\infty} L_{n\downarrow} = \sum_{n=1}^{\infty} \frac{1}{n} \int_0^x x'^n \exp(-\alpha x')\, \mathrm{d}x'; \quad 0 < x \le 1. \tag{10}$$

The integral $L_{n\downarrow}$ of (10) cannot be solved directly, but for $n = 1$ we find

$$L_{1\downarrow} = \frac{1 - t(1 + \beta)}{\alpha^2}, \tag{11}$$

where $t = e^{-\beta}$. For $n > 1$, the following recurrence relation can be found:

$$L_{n\downarrow} = \frac{-t x^n}{\alpha n} + \frac{1}{\alpha} \int_0^x x'^{n-1} \exp(-\alpha x')\, \mathrm{d}x' = \frac{-t x^n}{n\alpha} + \frac{n-1}{\alpha} L_{n-1,\downarrow}. \tag{12}$$

Instead of directly computing $L_{n\downarrow}$, it is advantageous to introduce $J_n = L_{n\downarrow}/t$. For this quantity we find the downward recurrence formula

$$J_{n-1} = \frac{x^n}{n(n-1)} + \frac{\alpha J_n}{n-1}. \tag{13}$$

Downward recurrence is used to get stable solutions from (13). Starting at $m = \max(n)$, we note that $\lim_{m\to\infty} \sum_{n=m}^{\infty} J_n = 0$, and so we have for the starting value

$$J_m = \frac{x^{m+1}}{m(m+1)}. \tag{14}$$

The remaining terms follow from (13).

We can now write for the downwelling brightness temperature at the tropopause:

$$T_{b1} = T_p(1 - e^{\beta - \alpha}) = (T_g - \Gamma z_p)(1 - e^{\beta - \alpha}) + T_c e^{\beta - \alpha}, \tag{15}$$

Please cite this article as: Schneebeli M, Mätzler C. A radiative transfer model for an idealized and non-scattering atmosphere and its application for ground-based remote sensing. JQSRT (2010), doi:10.1016/j.jqsrt.2010.10.018

with the brightness temperature of the cosmic microwave background T_c. Inserting (15) into (7) leads to

$$T_{b\downarrow} = T_g(1-e^{-\alpha}) - \Gamma z_p(e^{-\beta}-e^{-\alpha}) - \Gamma z_0 \alpha L_\downarrow(\alpha,x) + T_c e^{-\alpha}. \quad (16)$$

An important quantity in ground-based remote sensing is the so-called mean tropospheric temperature or effective mean temperature T_{eff} [6,7]. It is defined as

$$T_{\text{eff}} = \frac{\int_0^\alpha T(\tau) e^{-\tau/\mu}\, d\tau}{1-e^{-\alpha}}. \quad (17)$$

With this definition, $T_{b\downarrow}$ can be written as

$$T_{b\downarrow} = T_{\text{eff}}(1-e^{-\alpha}) + T_c e^{-\alpha}. \quad (18)$$

From (18) and (16) we get the following expression for the effective mean temperature:

$$T_{\text{eff}} = T_g - \Gamma z_0 \left[\frac{z_p(e^{-\alpha x}-e^{-\alpha}) + \alpha z_0 L_\downarrow(\alpha,x)}{z_0(1-e^{-\alpha})}\right]. \quad (19)$$

2.2. Examples

We show two examples of how the previously derived expressions provide insight in the angular dependence of important observables in ground-based remote sensing. The upper panel of Fig. 1 shows the brightness temperature as a function of the zenith angle derived from Eq. (16). We have chosen values for $\gamma_a(0)$ and z_0 to parallel typical values for the frequencies of 52.5 and 54 GHz. With the relations $\alpha = \gamma_a(0) \cdot z_0$, $\beta = \alpha(1-\exp(-z_p/z_0))$ and $x = \beta/\alpha$ and the definition of z_p=12 000 m, $\Gamma = 6.5$ K km^{-1} and T_g=291 K everything is provided to draw the plot in question. The angular behavior of the brightness temperatures and their almost solely dependence on the temperature of the lower troposphere is nowadays widely used in retrieving tropospheric temperature profiles with microwave radiometers [17,11].

The lower panel of Fig. 1 shows the mean tropospheric temperature as a function of the zenith angle derived from Eq. (19). For this plot, values for $\gamma_a(0)$ and z_0 are chosen to parallel values for the frequencies of 22 and 31 GHz. The slight angular dependence is in agreement to the findings in Martin [10].

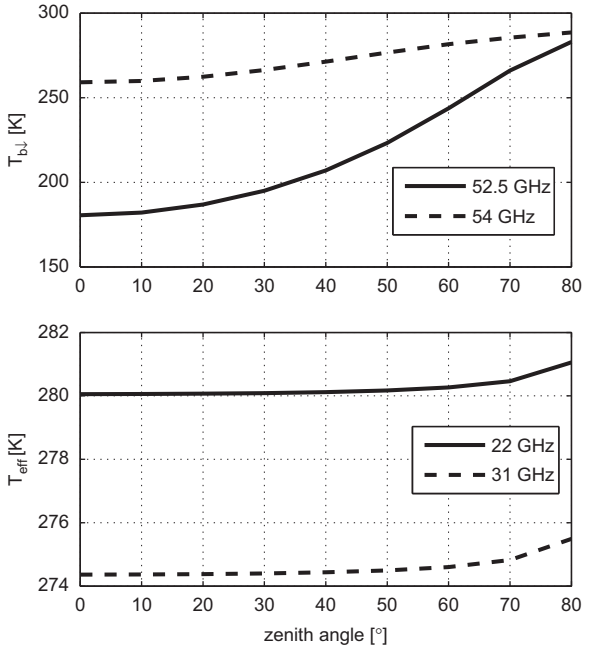

Fig. 1. Upper panel: Angular dependence of $T_{b\downarrow}$ at 52.5 and 54 GHz. Parameters used in the computations are: T_g=291 K, $\Gamma = 6.5$ K/km, z_p=12 km, 52.5 GHz: $\gamma_0 = 0.18$/km, z_0=6.4 km. 54 GHz: $\gamma_0 = 0.48$/km, z_0=6.0 km. Lower panel: Angular dependence of the effective tropospheric temperature at 22 and 31 GHz. Parameters used in the computations are: T_g=285 K, $\Gamma = 6.5$ K/km, z_p=12 km, 22 GHz: $\gamma_0 = 0.045$/km, z_0=1.8 km, 31 GHz: $\gamma_0 = 0.022$/km, z_0=2.7 km.

3. Adaption to realistic atmospheres

The real atmosphere does not exactly follow the simple assumptions of Section 2. We illustrate this in Fig. 3 where we calculated the absorption coefficient for radiosoundings made during six years in October and November at the station in Oppin, Germany. Calculations were made at frequencies that are typically used in ground-based tropospheric remote sensing applications (18, 22, 31, 52.5, 55, 90, 150 GHz). In addition, we fitted the exponential model given in Eq. (1) to the averaged absorption coefficient profile. It is seen that for certain frequencies, the absorption coefficient closely follows the exponential function but for others it does not. This is explained in the fact that some atmospheric tracers like water vapor do not decay exponentially with height, especially in the planetary boundary layer, wherefore the absorption coefficients being sensitive to such tracers also do not exhibit an ideal exponential behavior. Furthermore, the absorption coefficient also depends on the temperature, which decays linearly with height in the troposphere, and therefore also causes the absorption coefficient to decay in a slightly non-exponential manner. It is therefore necessary, as in every RT code, to discretize the atmosphere. First we start with profiles defined at discretized height levels $z_i, i = 1 \ldots N$ of T and γ_a. Then the model parameters are fitted within each layer separately. Since the model is adapted to the generic

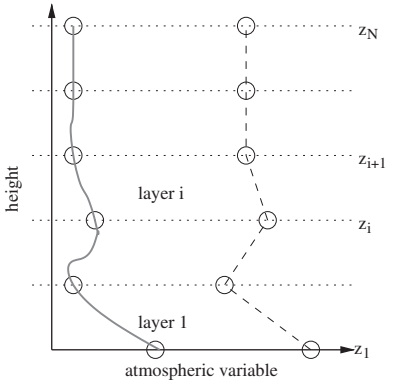

Fig. 2. Sketch of a real (gray line) and interpolated (dashed line) atmospheric profile (e.g. temperature or humidity measured with a radiosonde) explaining the denotation of the term 'layer' and grid points i. Height levels are denoted with z_i.

Please cite this article as: Schneebeli M, Mätzler C. A radiative transfer model for an idealized and non-scattering atmosphere and its application for ground-based remote sensing. JQSRT (2010), doi:10.1016/j.jqsrt.2010.10.018

behavior of the atmosphere, the number of layers needed is smaller than for models with constant values within each layer. A sketch of the discretized atmosphere that explains the terms 'layer' and 'height level' is shown in Fig. 2.

The absorption coefficient $\gamma_{a,i+1}$ at the upper boundary of the layer i is related to the value at the lower boundary with

$$\gamma_{a,i+1} = \gamma_{a,i} e^{-((z_{i+1}-z_i)/z_{0,i})}. \tag{20}$$

From this, the scale height $z_{0,i}$ of the layer i can be calculated as

$$z_{0,i} = -\frac{z_{i+1}-z_i}{\ln\left(\dfrac{\gamma_{a,i+1}}{\gamma_{a,i}}\right)}. \tag{21}$$

The zenith opacity of layer i reads

$$\tau_{p,i} = \int_{z_i}^{z_{i+1}} \gamma_a(z')\,\mathrm{d}z'. \tag{22}$$

We express $\gamma_a(z')$ with Eqs. (1) and (21) as

$$\gamma_a(z') = \gamma_{a,i} \exp\left(\frac{z' \ln\left(\dfrac{\gamma_{a,i+1}}{\gamma_{a,i}}\right)}{z_{i+1}-z_i}\right), \tag{23}$$

and solve the integral of Eq. (22) to get

$$\tau_{p,i} = \frac{\gamma_{a,i}(z_{i+1}-z_i)}{\ln\left(\dfrac{\gamma_{a,i+1}}{\gamma_{a,i}}\right)}\left[\frac{\gamma_{a,i+1}}{\gamma_{a,i}} - 1\right]. \tag{24}$$

According to the previous section, we define $\beta_i = \tau_{p,i}/\mu$, $x_i = \tau_{p,i}/\tau_{\infty,i}$ and $\alpha_i = \tau_{\infty,i}/\mu$ where $\tau_{\infty,i} = \gamma_{a,i} z_{0,i}$. Furthermore, $T_i = T(z_i)$ is the temperature at height level z_i. We have now everything to write the discretized form of Eq. (7)

$$T_{b\downarrow,i} = T_{b\downarrow,i+1} e^{-\beta_i} + T_i(1-e^{-\beta_i}) - \alpha_i \left(\frac{T_{i+1}-T_i}{\ln\left(\dfrac{\gamma_{a,i+1}}{\gamma_{a,i}}\right)}\right) L_\downarrow(\alpha_i, x_i). \tag{25}$$

For the calculation of the brightness temperature of the uppermost layer, the layer opacity is $\tau_{p,\max(i)} = z_{0,\max(i)}\gamma_{a,\max(i)}$, with the scale height $z_{0,\max(i)}$ to be chosen from a standard atmosphere. In addition, we have the relation $\tau_{\infty,\max(i)} = \tau_{p,\max(i)}$ and therefore $x_{\max(i)} = 1$. The brightness temperature at the top of the computational grid then follows directly from Eq. (7):

$$T_{b\downarrow,l} = T_c e^{-\alpha_l} + T_l(1-e^{-\alpha_l}) - \Gamma_l z_{0,l} \alpha_l L_\downarrow(\alpha_l, 1), \tag{26}$$

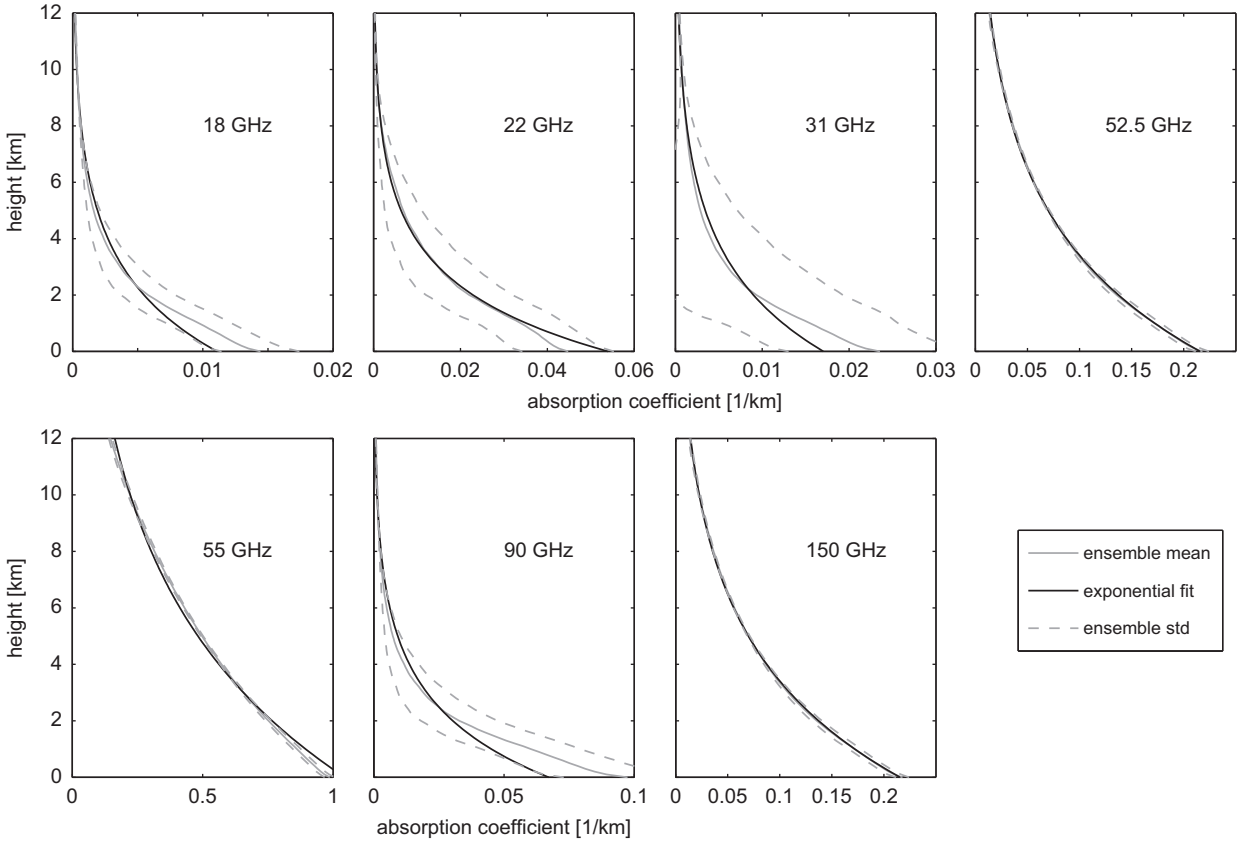

Fig. 3. Absorption coefficient profiles and corresponding standard deviation borders calculated for an ensemble of radiosoundings made in October and November during six years (2000–2005) at the station in Oppin, Germany. The exponential model from Eq. (1) is fitted to every mean profile.

Please cite this article as: Schneebeli M, Mätzler C. A radiative transfer model for an idealized and non-scattering atmosphere and its application for ground-based remote sensing. JQSRT (2010), doi:10.1016/j.jqsrt.2010.10.018

with l=max(i), the temperature gradient Γ_l and the cosmic microwave background T_c. If x=1, the convergence of $L_\downarrow(\alpha,x)$ is slow, so either a very large m has to be selected as the starting value for the recurrence, or the function needs to be approximated:

$$L_\downarrow(\alpha,x=1)\approx\begin{cases}\exp\left(-\dfrac{0.794\alpha}{1+0.0677\alpha}\right); & 0\le\alpha\le 6,\\ \exp\left(-0.692-\dfrac{0.649\alpha}{1+0.0732\alpha}\right); & 6<\alpha<40.\end{cases} \tag{27}$$

The standard deviation of the upper fit is 1.4% and 2% for the lower one.

In order to speed up RT calculations, an approximation formula for $L_\downarrow(\alpha,x)$ was also developed for $0\le x<1$. The following polynomial ansatz was empolyed:

$$L_\downarrow(\alpha,x)=\sum_{k=0}^{3}a_i(\alpha)x^i. \tag{28}$$

For several values of x and α, the a_i coefficients are fitted in a least square sense. By looking at the fitted coefficients, it is seen that these coefficients are related to functions of the form:

$$a_i(\alpha)=c_1(\alpha-c_2)+c_3\{c_4\cos(\alpha-c_2)e^{-c_5(\alpha-c_2)}+c_3\}-c_7. \tag{29}$$

As before, c_i were evaluated with a least square fit. The resulting coefficients are given in Table 1. In Fig. 4 the approximated $L_\downarrow(\alpha,x)$ is drawn together with the difference to the real $L_\downarrow(\alpha,x)$ function from Eq. (11).

The brightness temperature intercepted at the surface, $T_{b\downarrow,1}$, results from the subsequent calculation of Eq. (25), with Eq. (26) acting as the starting value. The calculation fails if $\gamma_{a,i+1}\ge\gamma_{a,i}$. In this case, the layer opacity can be calculated as $\tau_{p,i}=\gamma_{a,i}(z_{i+1}-z_i)$ and the effective mean temperature is the mean temperature of the layer, $T_{\mathrm{eff}}=(T_{i+1}+T_i)/2$, such that the downwelling brightness temperature can be expressed as

$$T_{b\downarrow,i}=T_{b\downarrow,i+1}e^{-\alpha_i x_i}+\frac{T_{i+1}+T_i}{2}(1-e^{-\alpha_i x_i}). \tag{30}$$

It must be mentioned that this situation only occurs if the discretization layers are sufficiently thin. Brightness temperature calculations through thin layers are only very weakly affected by discretization errors, wherefore the exceptional usage of Eq. (30) instead of Eq. (25) should not hamper the performance of the proposed model. Also note that, in contrast to the absorption coefficient, the model remains valid even if $T_{i+1}\ge T_i$.

For large zenith angles, the curvature of the earth has a considerable impact on the modeling of microwave brightness temperatures [6]. We therefore derived functions for calculating an effective value of the cosine of the zenith angle, $\mu_{\mathrm{eff},i}$, at every grid point i. The results are found in Schneebeli and Mätzler [15].

Table 1
The coefficients c_i used in Eq. (29) for fitting the $L_\downarrow$-function.

	c_1	c_2	c_3	c_4	c_5	c_6	c_7
a_1	0	−1.0207	0.9078	0.5783	0.8306	1.3034	−0.022
a_2	0	−2.9606	−2.6181	0.4374	0.7489	1.9746	0.0752
a_3	−0.0088	−2.6025	1.1809	0.44	0.9043	1.5831	−0.1639
a_4	0.0007	−4.2149	0.76	0.8453	1.1103	1.1622	0.0115

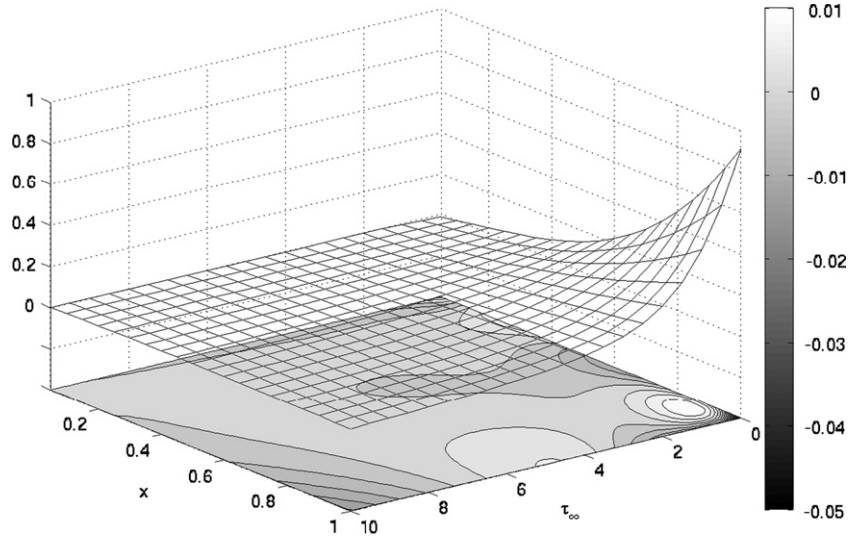

Fig. 4. The approximated $L_\downarrow(\tau_\infty,x)$ (grid surface) and the difference to the real function (contoured surface on the bottom).

Please cite this article as: Schneebeli M, Mätzler C. A radiative transfer model for an idealized and non-scattering atmosphere and its application for ground-based remote sensing. JQSRT (2010), doi:10.1016/j.jqsrt.2010.10.018

4. Validation and comparison

In this section, it will be tested how accurately brightness temperatures can be modeled with the new RT scheme (NRT) defined in the previous section. The accuracy is assessed in two experiments: In the first experiment, a radiosonde profile of pressure, temperature and humidity measurements is interpolated with the nearest neighbor method on an equally spaced discretization grid. The grid spans from a height of 0–30 km, and brightness temperature calculations are performed for varying distances between the grid points.

In the second experiment, NRT is applied on smoothed radiosonde profiles that are defined on a grid with grid point distances increasing exponentially with height. Such a grid is advantageous for calculating the intercepted radiation at the surface, since the lower atmospheric layers contribute more to the downwelling brightness temperatures than the higher

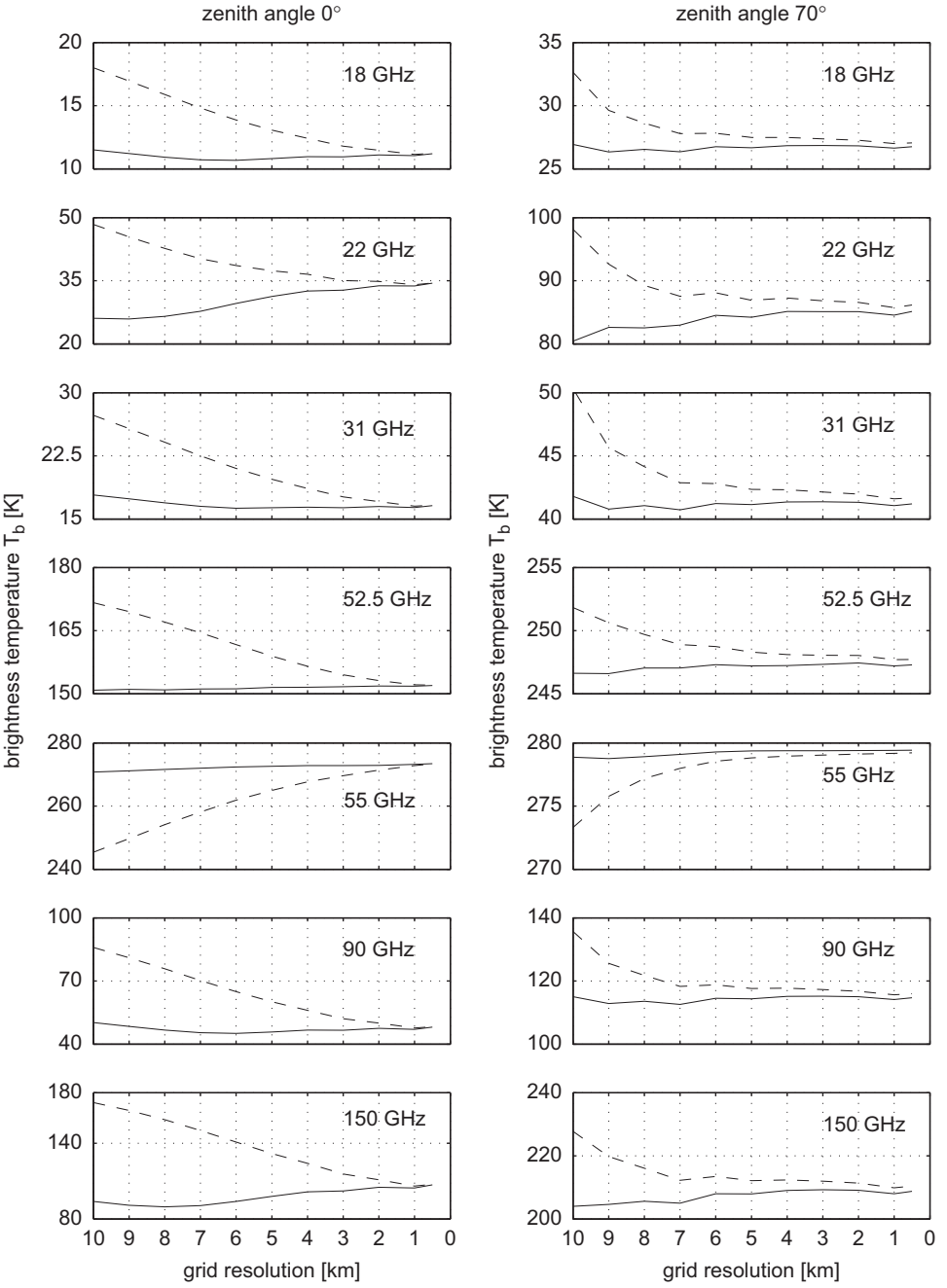

Fig. 5. Modelled brightness temperatures at frequencies indicated in the figure obtained with NRT (solid lines) and ORT (dashed lines). The meteorological profile data stem from the Payerne radiosounding of February 12, 2007, 12 UTC. The spacing of the calculation grid was varied from 10 km to 500 m. The zenith angle used in the calculations was 0° for the left panels and 70° for the right panels.

Please cite this article as: Schneebeli M, Mätzler C. A radiative transfer model for an idealized and non-scattering atmosphere and its application for ground-based remote sensing. JQSRT (2010), doi:10.1016/j.jqsrt.2010.10.018

levels. The radiosonde profiles were smoothed because we want to assess the modeling accuracy for atmospheric profiles as they are obtained from a profile retrieval technique. Radiometrically retrieved profiles do not exhibit small scale variations, wherefore brightness temperature calculations are less sensitive to the discretization of the profiles.

For comparison, RT calculations for the two experiments were also performed with an 'ordinary' RT scheme, as it is employed in most commonly used radiative transfer codes, e.g. Bühler et al. [1]. The definition of the 'ordinary' RT scheme (ORT) was already given with Eq. (30). The calculations were made at seven frequencies (18, 22, 31, 52.5, 55, 90, 150 GHz) and at two zenith angles (0° and 70°). Absorption coefficients were obtained with the model of Rosenkranz [13].

4.1. Linear grid

An example of RT calculations made with an equally spaced grid and applied to a radiosounding from Payerne is shown in Fig. 5. The brightness temperatures modeled with the NRT and ORT scheme converge toward a common value when the grid becomes finer. As expected, the NRT model results converge faster than the ORT model results. At 31 and 55 GHz, it seems that convergence is already reached for a grid resolution of 5 km albeit this is a more qualitative judgement based on only one radiosounding profile. The 22 GHz brightness temperature on the other hand seems to converge more slowly. The general shape of the convergence curves is similar for both zenith angles.

We know from Fig. 3 that for certain frequencies the assumption of an absorption coefficient decreasing exponentially with height is not entirely true, with the result that distortions in the shape of the spectral lines are expected if they are modeled with NRT. In line window regions, the exponential assumption is expected to be more accurate than in the line center, especially if water vapor lines are considered. We therefore calculated a whole brightness temperature spectrum from 10 to 150 GHz with NRT at a grid resolution of 5 km and as reference with ORT at a grid resolution of 500 m. The results of these calculations are given in Fig. 6. It is seen that the relative differences to the reference brightness temperature spectrum are largest at the center of the 22 GHz water vapor line as well as in the window regions around 100 GHz and above 130 GHz. These window regions are heavily influenced by the wing of the very strong 183 GHz water vapor line, which explains the differences to the reference calculations. Other window regions (below 18 GHz and around 30 GHz), that are not under the influence of the 183 GHz wing, exhibit good agreement with the reference spectrum. In the center of the oxygen complex around 55 GHz we also note a disagreement between the two calculations. Since the air in this frequency region is almost a black body, inaccuracies in the modeling of the air temperature profile leads to differences in brightness temperatures.

4.2. Exponential grid

An adapted discretization grid is introduced, with height levels that are defined as

$$z_i = C(e^{\mathbf{v}_{np}} - 1), \tag{31}$$

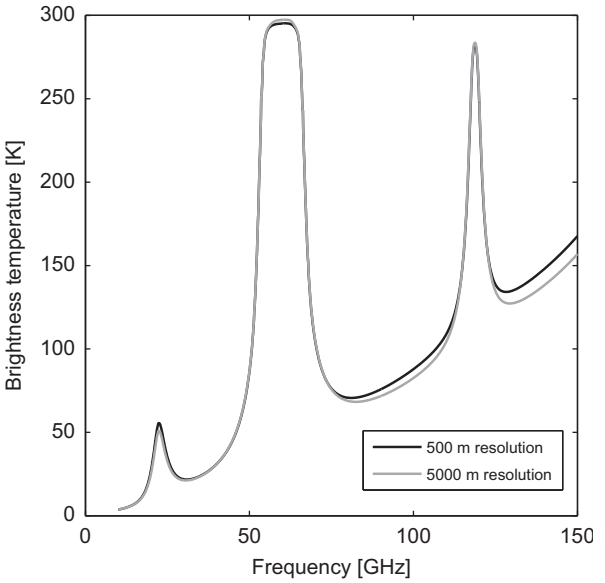

Fig. 6. Brightness temperature spectrum calculated with ORT at a resolution of 500 m and with NRT at a resolution of 5 km. The calculations were made for the radiosounding made in Oppin, Germany on September 9, 2005, 12 UTC.

where C is a constant and $\mathbf{v}_{np}$ is a vector defined as

$$\mathbf{v}_{np} = \left[0, \frac{1D}{np-1}, \frac{2D}{np-1}, \ldots, D\right]. \tag{32}$$

Hereby, np denotes the number of grid points and D is a constant to be chosen. The higher the value for D, the denser is the grid in the lower part of the atmosphere. We set D to a value of three, resulting in an adapted grid that corresponds to the retrieval grid used in Martin et al. [11]. The constant C needs to be adapted such that the uppermost height level equals 30 km. For our choice of D, C is determined to a value of 1.57 for z_i values given in kilometers.

Smoothed profiles are obtained by convolving radiosonde profiles with the averaging kernel of a retrieved profile. According to Tsou et al. [16], a smoothed profile vector is obtained with

$$\mathbf{p}_s = \mathbf{p}_a + \mathrm{A}(\mathbf{p}_{rs} - \mathbf{p}_a), \tag{33}$$

where $\mathbf{p}_a$ is the a-priori profile of the radiometer profile retrieval, $\mathbf{p}_{rs}$ is the radiosonde profile and A is the averaging kernel matrix of the retrieval. The applied profile retrieval, detailed in Schneebeli [14], calculates temperature and humidity profiles simultaneously. By applying Eq. (33) on a profile vector that contains temperature and humidity measurements from a radiosonde, smoothed temperature and humidity profiles are obtained. In order to get an ensemble of smoothed profiles, we performed retrieval simulations similar to the description given in Schneebeli [14], with the difference that a retrieval grid with very high resolution of 60 m was used. The retrieval simulation was based on radiosonde profiles from the station in Oppin, Germany.

Fig. 7 shows an example of modeled brightness temperatures similar to those given in Fig. 5, but with smoothed profiles underlying the RT calculations instead

Please cite this article as: Schneebeli M, Mätzler C. A radiative transfer model for an idealized and non-scattering atmosphere and its application for ground-based remote sensing. JQSRT (2010), doi:10.1016/j.jqsrt.2010.10.018

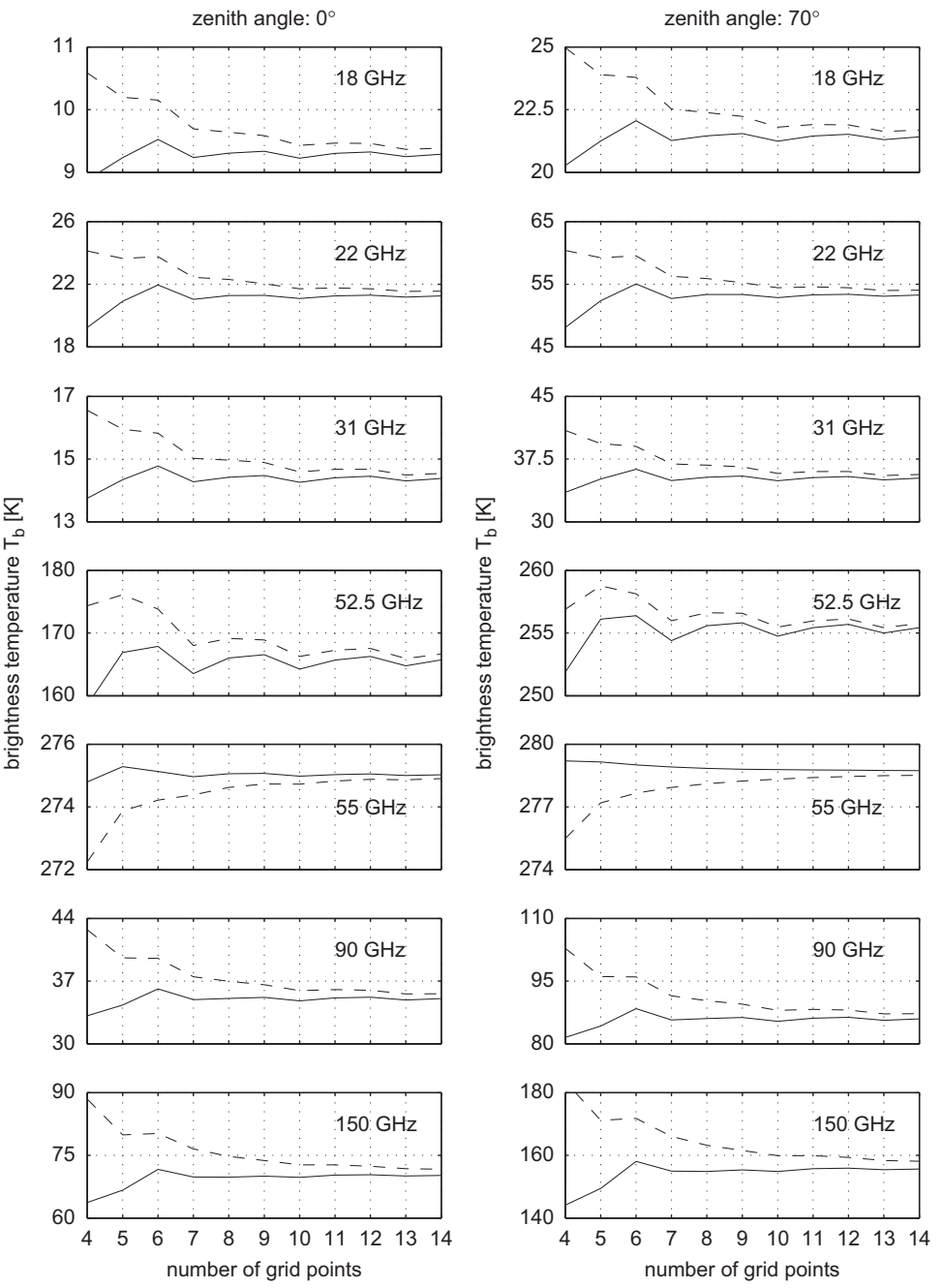

Fig. 7. Similar to Fig. 5, but a smoothed radiosonde profile from the Oppin station measured on September 4, 2007, 12 UTC was used. Brightness temperatures were calculated on the adapted grid given in Eq. (31).

of original radiosonde profiles. The smoothed profiles were interpolated with the nearest neighbor method on the retrieval grid given in Eq. (31). In the example shown, brightness temperatures calculated with the NRT model on a grid of seven points already converge for most frequencies. However, some oscillations are observed for calculations made with more grid points. Brightness temperatures at a frequency of 52.5 GHz seem to be very dependent on the number of grid points and exhibit the most oscillatory behavior, which is probably due to the choice of the exponential calculation grid.

The performance of the NRT and the ORT schemes were assessed by applying the two models to an ensemble of 90 smoothed radiosonde profiles from September and October 2005 at the Oppin radiosonde station. Brightness temperatures were calculated with the same number of grid points as in the example given in Fig. 7. An additional calculation with 50 grid points provided the 'true' brightness temperature

Please cite this article as: Schneebeli M, Mätzler C. A radiative transfer model for an idealized and non-scattering atmosphere and its application for ground-based remote sensing. JQSRT (2010), doi:10.1016/j.jqsrt.2010.10.018

Table 2
The brightness temperature mean difference as absolute value with respect to the true value for an ensemble of calculations made with the indicated number of grid points (GP). Smoothed profiles and the exponential calculation grid were used. Zenith angle is 0°.

Frequency (GHz)	RT model	Brightness temperature mean difference (K)					
		4 GP	6 GP	8 GP	10 GP	12 GP	14 GP
18	NRT	0.44	0.22	0.043	0.061	0.052	0.016
	ORT	1.7	0.98	0.43	0.19	0.21	0.13
22	NRT	2.6	0.59	0.20	0.34	0.085	0.065
	ORT	4.0	2.8	1.2	0.51	0.55	0.36
31	NRT	0.62	0.40	0.089	0.097	0.10	0.030
	ORT	2.9	1.6	0.72	0.29	0.35	0.21
52.5	NRT	6.9	2.1	0.33	1.46	0.53	0.035
	ORT	8.8	8.0	3.4	0.47	1.73	0.86
55	NRT	1.8	0.88	0.55	0.45	0.31	0.24
	ORT	4.3	1.6	0.89	0.65	0.43	0.32
90	NRT	2.4	1.0	0.25	0.25	0.29	0.11
	ORT	10	5.3	2.4	1.2	1.2	0.75
150	NRT	7.6	1.2	0.72	0.68	0.41	0.22
	ORT	23	11	5.4	3.0	2.5	1.7

Table 3
The same as in Table 2 but for calculations made with a zenith angle of 70°.

Frequency (GHz)	RT model	Brightness temperature mean difference (K)					
		4 GP	6 GP	8 GP	10 GP	12 GP	14 GP
18	NRT	1.2	0.58	0.11	0.16	0.14	0.044
	ORT	4.7	2.7	1.2	0.52	0.57	0.35
22	NRT	6.4	1.4	0.46	0.80	0.19	0.15
	ORT	9.2	6.6	2.9	1.2	1.3	0.85
31	NRT	1.6	1.0	0.2	0.25	0.27	0.07
	ORT	7.4	4.3	1.9	0.78	0.93	0.54
52.5	NRT	4.3	0.58	0.21	0.90	0.13	0.14
	ORT	0.95	2.4	1.0	0.19	0.55	0.22
55	NRT	1.5	1.3	1.0	0.76	0.65	0.51
	ORT	5.2	2.3	1.4	0.93	0.73	0.54
90	NRT	5.2	2.1	0.51	0.54	0.61	0.22
	ORT	21	11	5.2	2.6	2.5	1.6
150	NRT	11	1.5	1.1	1.0	0.49	0.33
	ORT	27.6	14.8	7.3	4.1	3.5	2.2

values. The absolute value of the mean difference between the 'true' brightness temperature and the brightness temperature calculated with fewer grid points was evaluated and the results are given in Tables 2 and 3 for RT calculations with a zenith angle of 0° and 70°, respectively.

The application of NRT reduces the mean difference to a large extent at all frequencies compared to ORT. For the brightness temperature calculations made with a zenith angle of 0°, the mean difference is reduced by a factor of 1.6 for the brightness temperatures at 55 GHz, by a factor of eight at 52.5 GHz and by a factor of five to seven for the other frequencies. The brightness temperature calculations made with a zenith angle of 70° exhibit similar factors of reduction, with the exception of the 52.5 GHz frequency where the mean difference is reduced by a factor of 2.5.

5. Discussion and conclusion

An analytic radiative transfer model for predicting microwave brightness temperatures intercepted at the surface was developed in the first part of this chapter. The model is based on the assumption of a linear temperature gradient up to the tropopause and an exponentially decaying absorption coefficient. The model output can be brought in agreement with observations by adjusting the temperature gradient and the absorption coefficient scale height.

In the second part, the analytic 'one-layer-model' was adapted to a more realistic behavior of the temperature and absorption coefficient profiles by separating the atmosphere into sub-layers. The downwelling brightness temperature of

Please cite this article as: Schneebeli M, Mätzler C. A radiative transfer model for an idealized and non-scattering atmosphere and its application for ground-based remote sensing. JQSRT (2010), doi:10.1016/j.jqsrt.2010.10.018

each sub-layer was calculated individually with the analytic RT model. With an iterative approach, the downwelling brightness temperature at the surface was readily obtained.

Since this new radiative transfer scheme takes the generic behavior of the atmosphere into account, accurate brightness temperature calculations are obtained with fewer layers compared to commonly used RT schemes. This was assessed by applying NRT on ORT to radiosonde profiles that were convolved with the averaging kernel of a radiometric temperature and humidity profile inversion technique. The convolution approach provided smoothed temperature and humidity profiles whose resolution correspond to the resolution of profiles retrieved from microwave measurements. It was found that NRT considerably reduces the brightness temperature difference that is introduced with the under-sampling of the underlying profiles. A reduction of the absolute value of the mean difference by a factor of six with respect to calculations made with ORT is obtained for almost all frequencies. The largest improvement was found for calculations made in zenith direction at 52.5 GHz. This frequency is almost ideal for the application of our model since (1) the mean absorption coefficient profile can be accurately described with the model given in Eq. (1); (2) there is a limited influence of water vapor; and (3) the brightness temperature does not too strongly depend on the (very variable) temperature profile of the boundary layer.

The error reduction is lower for brightness temperatures at 55 GHz. The reason of the limited improvement is explained in the fact that the brightness temperature at this frequency depends almost exclusively on the temperature profile of the lowermost first kilometer of the atmosphere and not on the profile of the absorption coefficient. The advantage of taking into account an exponentially decaying absorption coefficient therefore vanishes and relatively large errors persist as long as the temperature profile in the boundary layer is not exactly represented in the model atmosphere.

The overall results suggest that NRT is a useful scheme for calculating brightness temperatures from smoothed atmospheric profiles. The inversion of atmospheric profiles is an application where such a scheme could be useful. Since convergence is achieved with fewer atmospheric layers, the time needed for calculating the weighting function matrix could be reduced. Furthermore, instead of using a profile retrieval grid that spans over the whole tropopause, a smaller grid could be used, with the brightness temperature that enters the uppermost layer to be modeled with NRT. In the article at hand, the effect of clouds has been neglected, which is inappropriate for an operational RT scheme. Therefore, further developments are necessary before NRT can be used for the suggested applications.

References

[1] Bühler SA, Eriksson P, Kuhn T, von Engeln A, Verdes C. ARTS, the atmospheric radiative transfer simulator. J Quant Spectrosc Radiat Transfer 2005;91:65–93.
[2] Cimini D, Hewison TJ, Martin L, Güldner J, Gaffard C, Marzano F. Temperature and humidity profile retrievals from ground-based microwave radiometers during TUC. Meteorol Z 2006;15:45–56.
[3] Cimini D, Westwater ER, Gasiewski AJ, Klein M, Leuski VY, Liljegren JC. Ground-based millimeter- and submillimeter-wave observations of low vapor and liquid water contents. IEEE Trans Geosci Remote Sens 2007;45:2169–80.
[4] Crewell S, Löhnert U. Accuracy of cloud liquid water path from ground-based microwave radiometry 2. Sensor accuracy and synergy. Radio Sci 2003;38:8042.
[5] Güldner J, Spänkuch D. Results of year-round remotely sensed integrated water vapor by ground-based microwave radiometry. J Appl Meteorol 1999;38:981–8.
[6] Han Y, Westwater ER. Analysis and improvement of tipping calibration for ground-based microwave radiometers. IEEE Trans Geosci Remote Sens 2000;38:1260–76.
[7] Ingold T, Peter R, Kämpfer N. Weighted mean tropospheric temperature and transmittance determination at millimeter-wave frequencies for ground-based applications. Radio Sci 1998;33:905–18.
[8] Janssen MA. An introduction to the passive microwave remote sensing of atmospheres. In: Janssen MA, editor. Atmospheric remote sensing by microwave radiometry. New York: Wiley; 1993. p. 1–35.
[9] Löhnert U, Crewell S. Accuracy of cloud liquid water path from ground-based microwave radiometry 1. Dependency on cloud model statistics. Radio Sci 2003;38:8041.
[10] Martin L. Microwave transmission and emission measurements for tropospheric monitoring. PhD thesis, University of Bern, Bern, Switzerland, available from 〈http://www.iap.unibe.ch/publications〉; 2003.
[11] Martin L, Schneebeli M, Mätzler C. Tropospheric water and temperature retrieval for ASMUWARA. Meteorol Z 2006;15:37–44.
[12] Melsheimer C, Verdes C, Bühler SA, Emde C, Eriksson P, Feist DG, et al. Intercomparison of general purpose clear sky atmospheric radiative transfer models for the millimeter/submillimeter spectral range. Radio Sci 2005;40:RS1007.
[13] Rosenkranz PW. Water vapor microwave continuum absorption: a comparison of measurements and models. Radio Sci 1998;33:919–28.
[14] Schneebeli M. Advancements in ground-based microwave remote sensing of the troposphere—calibration, data retrieval and applications. PhD thesis, University of Bern, Bern, Switzerland, available from 〈http://www.iap.unibe.ch/publications〉; 2009.
[15] Schneebeli M, Mätzler C. Radiometer calibration and radiative transfer modeling for ASMUWARA. Research Report 2008-03-MW, Institute of Applied Physics, University of Bern, Bern, Switzerland, available from 〈http://www.iap.unibe.ch/publications〉; 2008.
[16] Tsou JJ, Connor BJ, Parrish A, McDermid IS, Chu WP. Ground-based microwave monitoring of middle atmosphere ozone: comparison to lidar and stratospheric aerosol and gas experiment II satellite observations. J Geophys Res 1995;100:3005–16.
[17] Westwater ER. Ground-based microwave remote sensing of meteorological variables. In: Janssen MA, editor. Atmospheric remote sensing by microwave radiometry. New York: Wiley; 1993. p. 145–213.
[18] Westwater ER, Crewell S, Mätzler C. A review of surface-based microwave and millimeter-wave radiometric remote sensing of the troposphere. Radio Sci Bull 2004;(3010):59–80.

Please cite this article as: Schneebeli M, Mätzler C. A radiative transfer model for an idealized and non-scattering atmosphere and its application for ground-based remote sensing. JQSRT (2010), doi:10.1016/j.jqsrt.2010.10.018